# Supplementary Material for: "3D-printed micro-axicon enables extended depth-of-focus intravascular optical coherence tomography *in vivo*"

**Pavel Ruchka[a], Alok Kushwaha[b,c], Jessica A. Marathe[d-f], Lei Xiang[b,c], Rouyan Chen[b,c,f], Rodney Kirk[c,d], Joanne T. M. Tan[d,f], Christina A. Bursill[d,f], Johan Verjans[d-f], Simon Thiele[g], Robert Fitridge[d,h], Robert A. McLaughlin[c,d], Peter J. Psaltis[d-f], Harald Giessen[a], and Jiawen Li[b,c,f*]**

[a] 4th Physics Institute and Research Center SCoPE, University of Stuttgart, 70569 Stuttgart, Germany
[b] School of Electrical and Mechanical Engineering, University of Adelaide, Adelaide, SA 5005, Australia
[c] Institute for Photonics and Advanced Sensing, University of Adelaide, Adelaide, SA 5005, Australia
[d] Faculty of Health and Medical Sciences, University of Adelaide, Adelaide, SA 5005, Australia
[e] Department of Cardiology, Central Adelaide Local Health Network, Adelaide, SA 5000, Australia
[f] Lifelong Health Theme, South Australian Health and Medical Research Institute (SAHMRI), Adelaide, SA 5000, Australia
[g] Institute of Applied Optics (ITO) and Research Center SCoPE, University of Stuttgart, 70569 Stuttgart, Germany
[h] Vascular and Endovascular Service, Central Adelaide Local Health Network, Adelaide, SA 5000, Australia
*Jiawen Li, jiawen.li01@adelaide.edu.au

**Table S1. Comparison of existing methods to create needle-beams in optical coherence tomography (OCT) probes.** The number of the references in the table below are consistent with the main manuscript.

| | How can it achieve a needle-beam | Disadvantages |
|---|---|---|
| Micro glass optics | Creating annual apodization by a hollow glass ferrule being angle-polished and gold-coated [18] | 1) Limited aperture size due to the complicated fabrication process of micro glass optics; 2) Non-monolithic structure, which tend to be subject to parasitic reflections |
| Fiber lens (e.g., GRIN fiber) the method that commonly used in commercial intravascular OCT devices | Molding a fiber into a micro-axicon [15] or generation of few-mode interferometry by utilizing a multimode fiber [6][19] | 1) Limited ability to correct astigmatism; 2) Limited aperture size because of the fiber being used |
| Meta lens or diffractive optical elements | Creating a phase masks [7] or generating tailored chromatic dispersion [4] | Difficulty in being directly integrated to fiber. It results in either a bulky imaging probe, or it can only be fabricated by 3D micro printing for near infrared or longer wavelength range; low efficiency of the meta-optics. |
| 3D printed micro-optics (e.g., micro-axicon) the method proposed in this manuscript | 3D printing directly on the fiber in a single step, as detailed in the methods section of this main manuscript | Limited capability in terms of polarization and chromatic engineering, which is not an issue for the application demonstrated in this manuscript and is not impossible to fabricate [36-37] |

## Beam-profile measurement

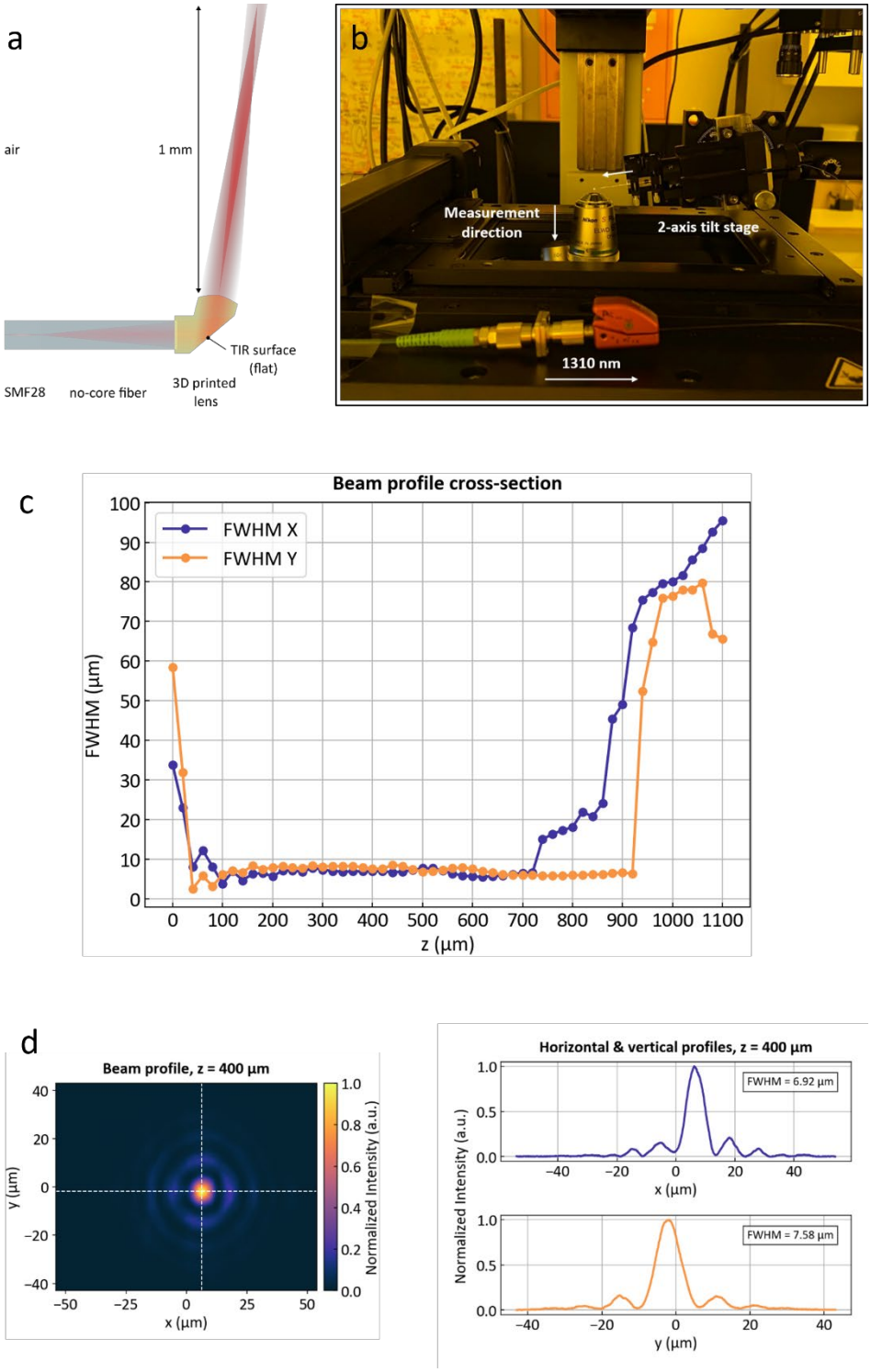


**Fig. S1.** Beam-profile measurement of the needle-beam probe. **a** Needle-beam optics design, adjusted for the measurement in air without the catheter sheath and a protective tube. We removed the catheters from the initial design and set the TIR surface to be flat, to single out and characterize the 3D-printed axicon lens. **b** Beam-profile measurement setup. We used NKT Extreme (NKT Photonics) laser at 1310 nm, coupled to the needle-beam fiber probe via Thorlabs BFT1 connector. The fiber probe was mounted in a home-built 2 axis tilt/rotation stage, which includes a rotating fiber holder. This stage allowed us the precise alignment of the beam with regard to the imaging optics. We used Nikon 60x S Plan Fluor (NA 0.7) in a Nikon Eclipse TE2000-U microscope setup to image the beam onto an IR-camera Alvium G1-130 VSWIR (Allied Vision GmbH). The pictures were taken manually each

20 µm by moving the microscope objective stage from the tip of the axicon downwards. **c** Full width half maximum values along horizontal (X) and vertical (Y) directions of the beam. The beam is focused starting from 40 µm until ca. 800 µm for both directions. The resolution remains fairly constant for both X and Y cross-sections well under 10 µm. **d** A single image of the beam at 400 µm distance from the axicon tip with the horizontal and vertical cross-sections through the highest intensity point. We observe a symmetrical shape with some Bessel-beam like rings around the focus, which is to be expected. The cross-sections show the FWHM resolution of 6.92 and 7.58 µm, respectively, with a rather symmetric spot shape.

## Confocal measurements

To evaluate the quality of the 3D printed surfaces we use confocal microscopy, which allows us to obtain the topography of the optically relevant surfaces with the resolution down to 7 nm.

For the measurements, the fiber with 3D printed lens is mounted in a fiber rotator (Thorlabs HFR007) on adjustable angle mounting plate (Thorlabs AP180/M with Thorlabs MMP1/M). Thus, we can pre-align the fiber and set the desired angle for the confocal measurement, so that the surface normal is aligned with the optical axis of the confocal microscope objective. We use a confocal microscope (nanofocus µsurf expert) with 50x objective (NA 0.95) to scan the surface. After the confocal scan, we extract the topology and the profiles of the measured surface. To avoid edge artefacts when evaluating and displaying data, we cut out surfaces, sacrificing few micrometers of the measured radius for each profile. We can also apply a spatial frequency filter to differentiate between waviness and surface roughness. For this, we use a cut-off frequency of 0.125 $\mu m^{-1}$. The resulting low spatial frequencies are considered as waviness and the high frequencies as the surface roughness.

We performed the measurements for the axicon surface and the biconical TIR surface as well.

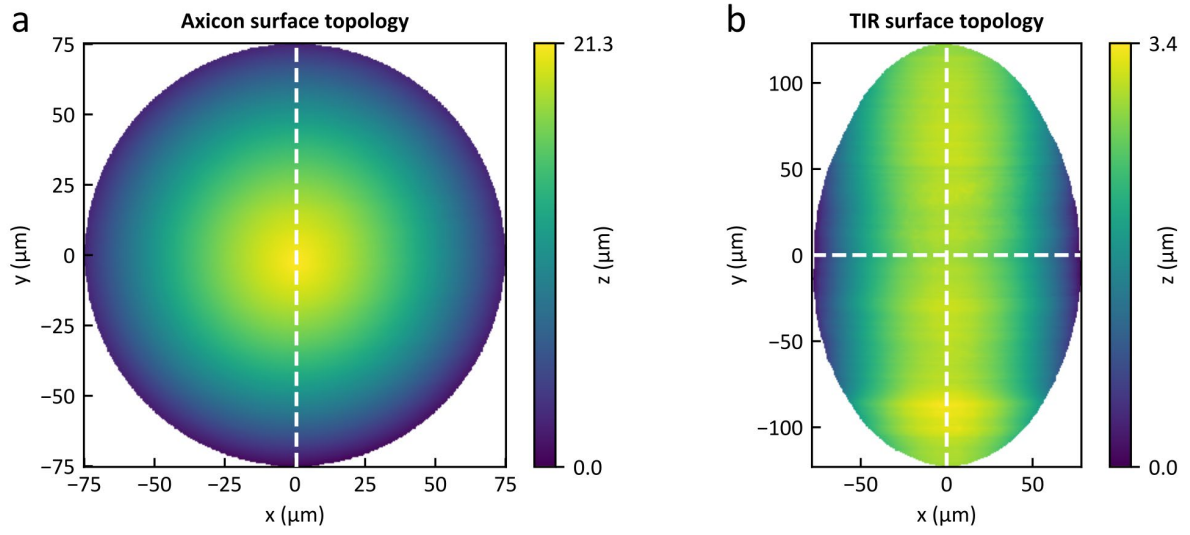


**Fig. S2**. Confocally measured topographies of the axicon (a) and TIR biconical surfaces (b). The white lines illustrate the cross-sections, which are shown in **Fig. S3**.

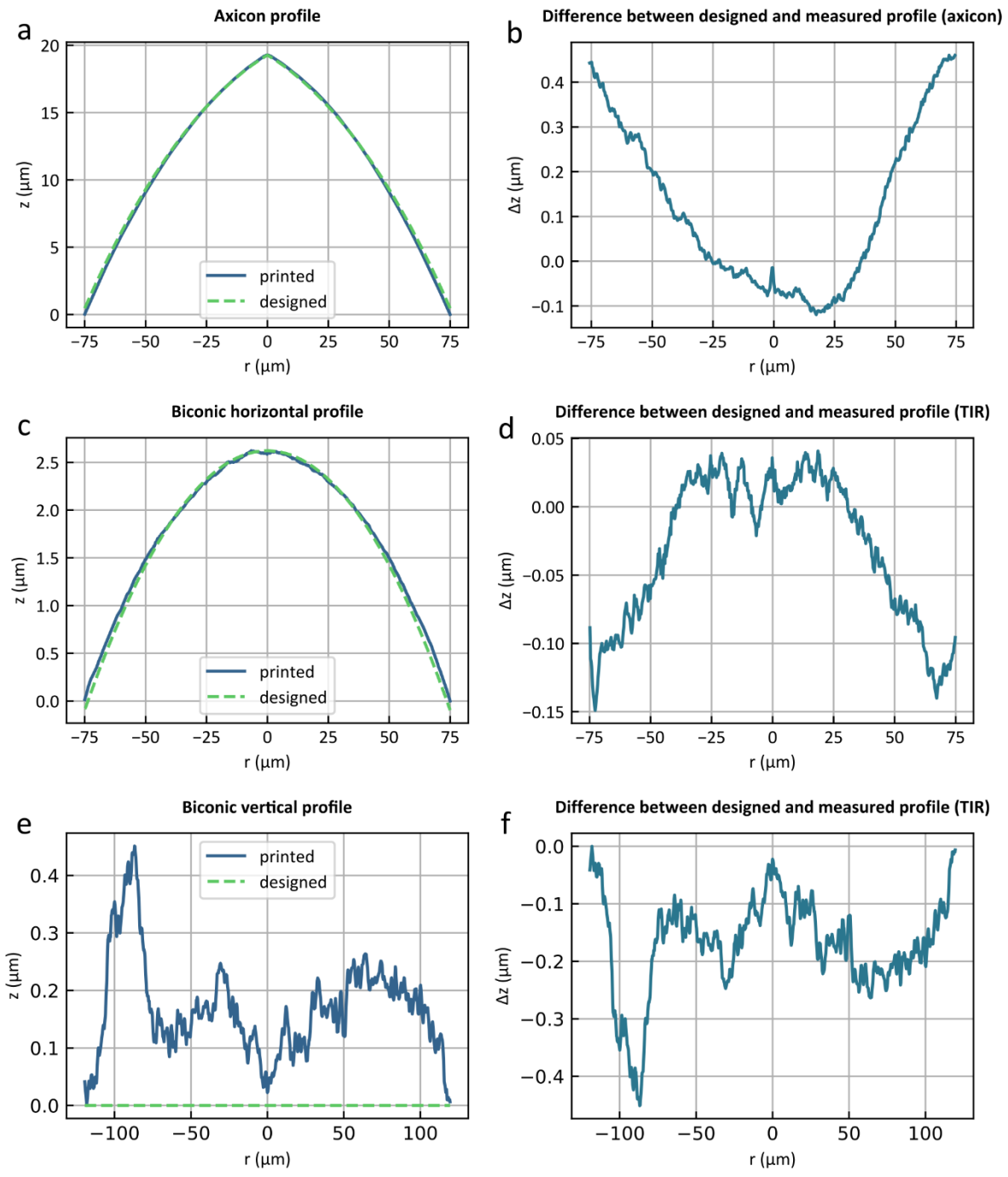


**Fig. S3.** Confocal profiles of the surfaces of the 3D printed needle-beam probe. **a** Measured axicon profile together with the designed profile. **b** Corresponding deviations between axicon design and measured profile. Peak-to-valley (P-V) deviation is less than 1 µm, hence we can assume that deviations do not affect the performance of the axicon significantly at our wavelength. **c** Measured profile of the biconical TIR surface vs designed profile (horizontal cross-section) with **d** depicting the corresponding deviations. The latter are less than 200 nm (P-V), hence we assume accurate printing of the optically relevant part of this surface. **e** Measured vertical profile of the biconical TIR surface vs corresponding design profile. **f** Difference between the profiles in **e**. Even with a peak in the left side of the surface, the overall P-V deviation is under 500 nm, therefore we again assume that the surface is printed with acceptable quality for our purposes, in particular for our working wavelength of 1.3 µm.

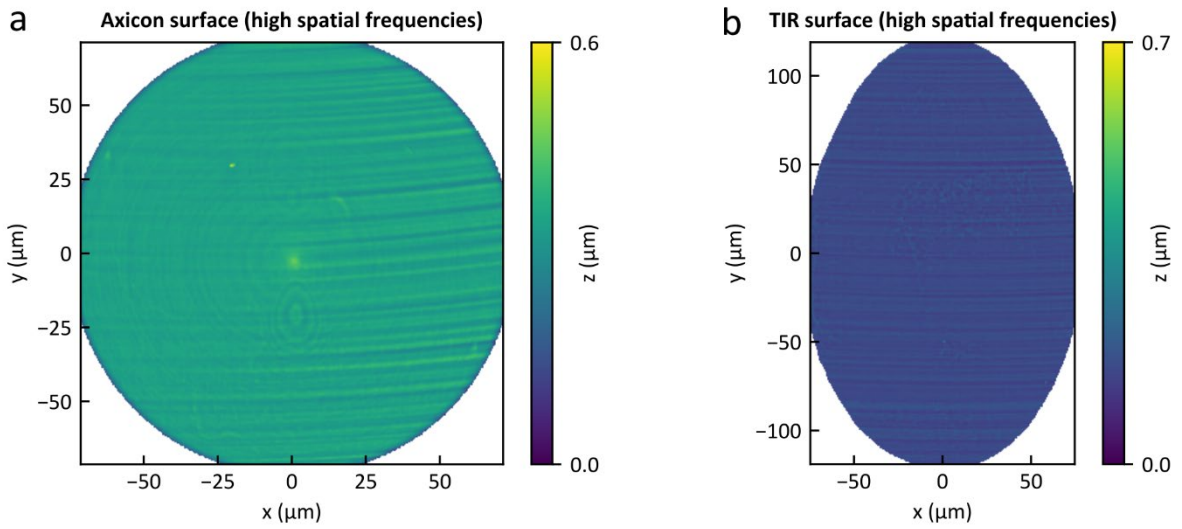


**Fig. S4.** Extracted high spatial frequency topographies of the axicon (a) and biconical TIR surface (b). The images depict spatial frequencies higher than 0.125 $\mu m^{-1}$. From these pictures we extract the roughness values of Sq = 32.5 nm and Sq = 14.3 nm respectively (with accordance to ISO 25178). The slightly washed-out part on the left-hand side in (a) may indicate a slight residue of a developer at the axicon surface, which smoothens the surface locally in a minor way.

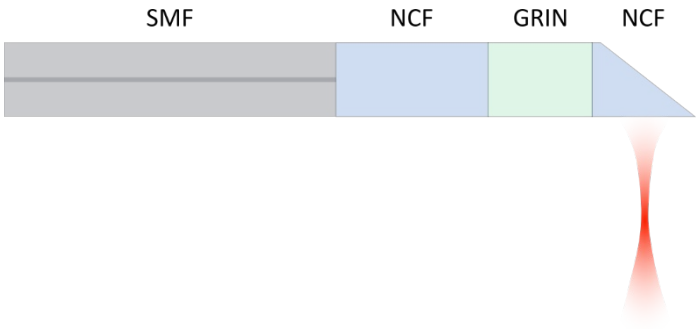


**Fig. S5.** Schematic of the GRIN probe. The gradient index (GRIN) fibre probe was created by splicing 350 µm long no-core fibre (NCF) and 145 µm long GRIN fibre onto a single-mode fibre (SMF, over 1.6 meter long) to create a nearly collimated beam. Then to enable side-viewing, a final NCF was spliced onto the GRIN fibre and then polished at 52 degrees to achieve total internal reflection at the NCF to air interface.

## Signal-to-noise ratio (SNR) measurement

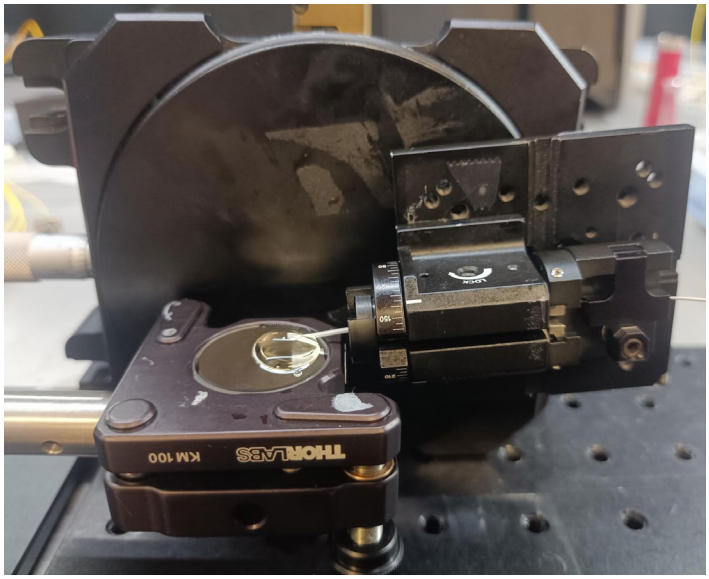


Fig. S6. Experiment setup for SNR measurement. The SNRs were measured for both the needle-beam and GRIN probe. Positioned approximately 550 µm from the catheter sheath (1 mm from the probe/air interface), a silver-coated mirror (PF10-03-P01, Thorlabs Inc., USA) was scanned using water-immersed probes. A 90:10 beam splitter (TW1300R2A1, Thorlabs Inc., USA) was placed in the sample arm to provide a 20 dB attenuation, preventing detector saturation. The SNR in dB was calculated according to Equation 1 [38],

$$SNR(dB) = 20\log\left(\frac{I_{mirror}}{\delta_{noise}}\right) + 20 \quad (1)$$

Where I_mirror is the peak A-scan intensity from the mirror and δ_noise is standard deviation of the noise floor, which was taken at the location of the mirror by blocking the sample arm.

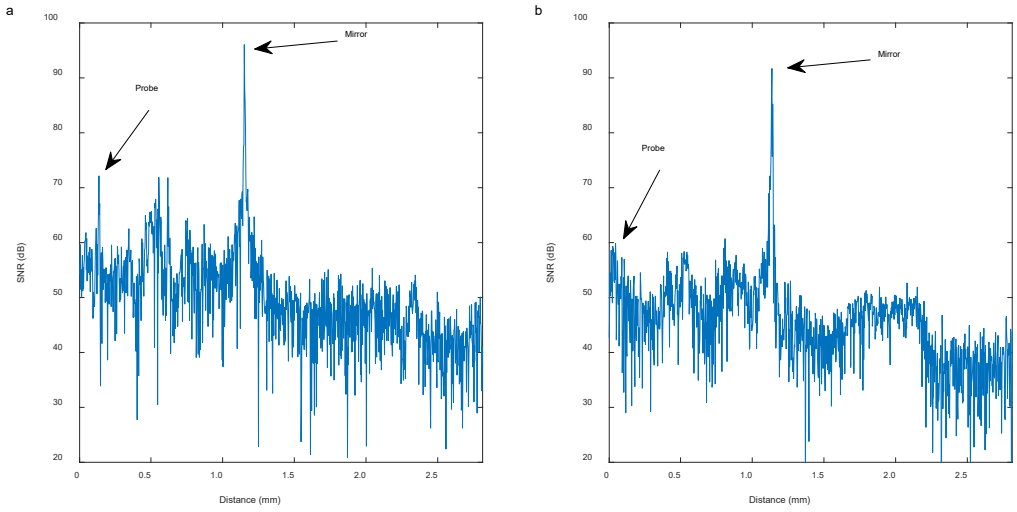


Fig. S7. Measured SNR of needle-beam probe and GRIN probe. (a) 3D-printed needle-beam probe; (b) GRIN probe; Probe, reflection from probe/air interface; Mirror, reflection from the silver-coated mirror. The measured SNR was 96.0 dB for the needle-beam probe and 91.7 dB for the GRIN probe. The difference between the two probes in terms of back-reflections can also be observed from these graphs.

## *Ex vivo* imaging of human plaques

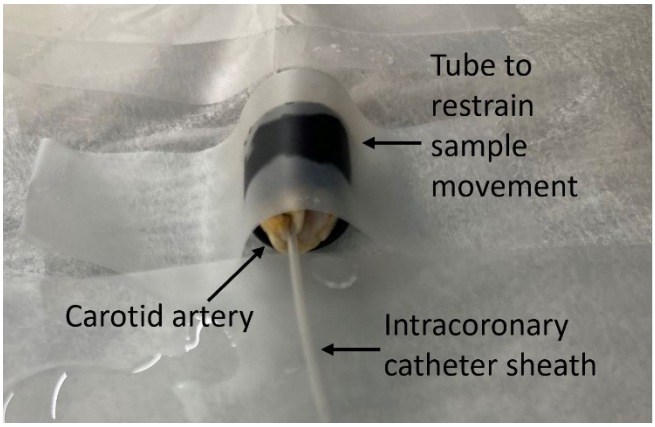


**Fig. S8.** Photo taken during the acquisition of OCT images of Figure 3. To ensure that the scans acquired with the 3D-printed and the GRIN fiber probes were co-located for comparison, the carotid artery was held inside a tube to restrain its movement. The outer intracoronary catheter sheath stayed inside the sample to ensure the probe always followed the same path for pullbacks.

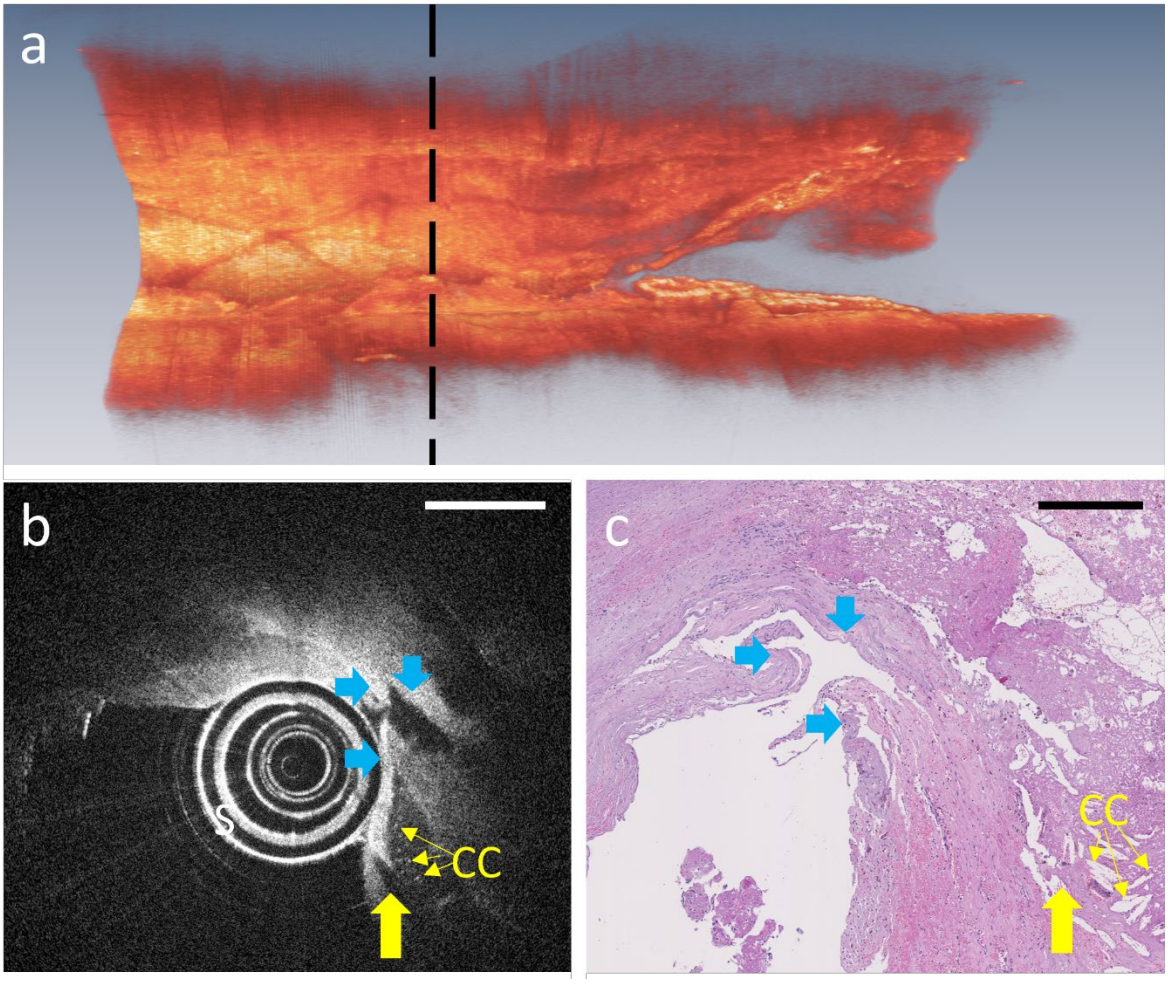


**Fig. S9.** *Ex vivo* imaging of a necrotic core in human carotid artery obtained by the 3D-printed needle-beam probe. **a** Three-dimensional rendering of the artery created by 225 frames of OCT images obtained with 3D-printed

needle-beam endoscopic probe. **b** Representative OCT image obtained at the black dashed line in **a** by the 3D-printed needle-beam endoscopic probe. **c** Corresponding H&E histology image. Inset: magnified view of the dashed line region. Blue arrows denote the landmark features used for matching needle-beam OCT and histology images; yellow arrow points to at the necrotic core region of the plaque. CC: cholesterol clefts. S: sheaths. Scale bar: 0.5 mm.

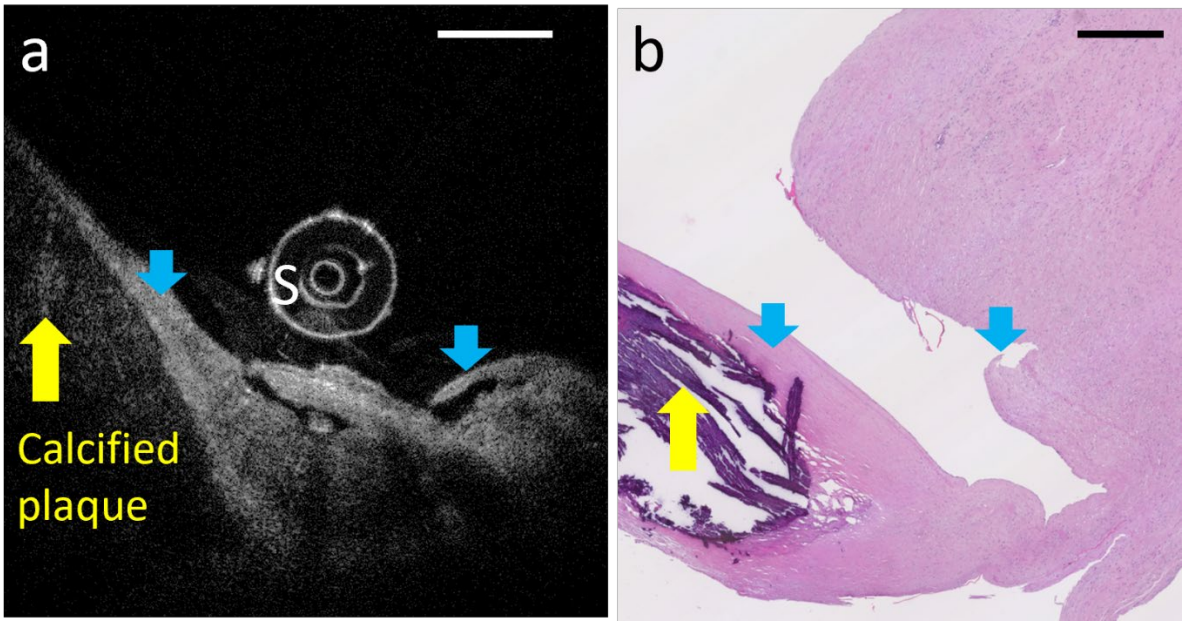


**Fig. S10.** *Ex vivo* imaging of a calcified plaque in human carotid artery obtained by the 3D-printed needle-beam probe. To illustrate the plaque features during the pull-back, OCT images were made into a video displaying at 15 frames per second (Movie S2). **a** Representative OCT image of the plaque. **b** Corresponding H&E histology image. Blue arrows denote the landmark features used for matching needle-beam OCT and histology images; yellow arrow points at the necrotic core. S: sheath. Scale bar: 0.5 mm.

## *In vivo* imaging of a swine across multiple time points

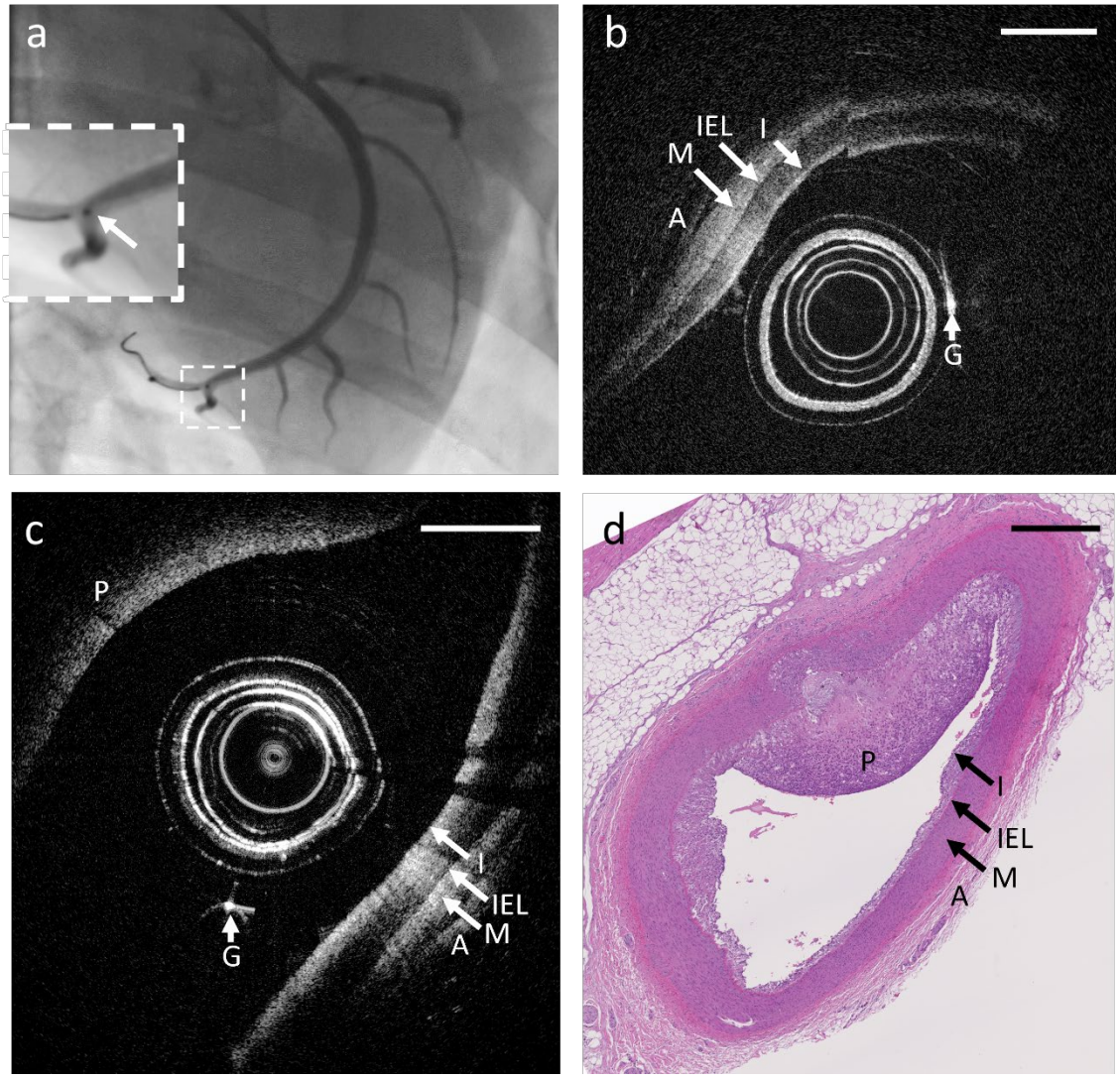


**Fig. S11.** *In vivo* imaging of swine circumflex coronary artery **a** X-ray angiography showing placement of the 3D-printed endoscopic probe in the distal circumflex artery, which is divided from the left coronary artery. Inset: magnified version with an arrow denotes the radiopaque marker at the tip of the 3D-printed needle-beam endoscopic probe; **b** Representative OCT image obtained in the circumflex coronary artery at the 3-month time point; **c** Representative OCT image obtained in the circumflex coronary artery at the 9-month time point; **d** Matching H&E histological image of the region imaged by **c**. I: intima; IEL: internal elastic lamina; A: adventitia; G: guidewire; P: plaque. Scale bar: 0.5 mm.